LANGMUIR Article
Cite This: *Langmuir* 2019, 35, 5484−5495
pubs.acs.org/Langmuir

Multilayer Formation in Self-Shaping Emulsion Droplets

Diana Cholakova,[†] Nikolai Denkov,*[,†] Slavka Tcholakova,[†] Zhulieta Valkova,[†] and Stoyan K. Smoukov[‡]

[†]Department of Chemical and Pharmaceutical Engineering, Faculty of Chemistry and Pharmacy, Sofia University, 1 James Bourchier Avenue, 1164 Sofia, Bulgaria

[‡]Active and Intelligent Materials Lab, School of Engineering and Materials Science, Queen Mary University of London, Mile End Road, London E14NS, UK

Supporting Information

ABSTRACT: In several recent studies, we showed that micrometer-sized oil-in-water emulsion droplets from alkanes, alkenes, alcohols, triglycerides, or mixtures of these components can spontaneously "self-shape" upon cooling into various regular shapes, such as regular polyhedrons, platelets, rods, and fibers (Denkov, N.,et al. *Nature* **2015**, *528*, 392; Cholakova, D.,et al. *Adv. Colloid Interface Sci.* **2016**, *235*, 90). These drop-shape transformations were explained by assuming that intermediate plastic rotator phase, composed of ordered multilayers of oily molecules, is formed beneath the drop surface around the oil-freezing temperature. An alternative explanation was proposed (Guttman, S.,et al. *Proc. Natl. Acad. Sci. USA* **2016** *113*, 493; Guttman, S.,et al. *Langmuir* **2017**, *33*, 1305), which is based on the assumption that the oil−water interfacial tension decreases to very low values upon emulsion cooling. Here, we present new results, obtained by differential scanning calorimetry (DSC), which quantify the enthalpy effects accompanying the drop-shape transformations. Using optical microscopy, we related the peaks in the DSC thermograms to the specific changes in the drop shape. Furthermore, from the enthalpies measured by DSC, we determined the fraction of the intermediate phase involved in the processes of drop deformation. The obtained results support the explanation that the drop-shape transformations are intimately related to the formation of ordered multilayers of alkane molecules with thickness varying between several and dozens of layers of alkane molecules, depending on the specific system. The new results provide the basis for a rational approach to the mechanistic explanation and to the fine control of this fascinating and industrially relevant phenomenon.

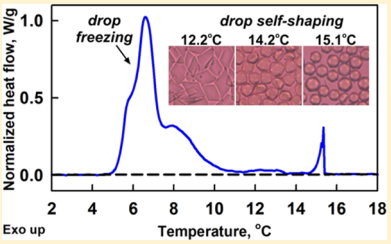

INTRODUCTION

Recently, we have shown[1−4] that micrometer-sized emulsion droplets, stabilized by long-chain surfactants, can spontaneously change their shape several times upon cooling, before the ultimate drop freezing (solidification). A general drop-shape evolution sequence was observed, in which the droplets first transform from spheres into fluid polyhedrons that gradually flatten and form hexagonal platelets. These hexagonal platelets can further evolve into either tetrangular platelets, which ultimately transform into rods and/or thin fibers, or triangular platelets, from the acute angles of which protrusions may grow, see Supporting Information Figure S1a. This phenomenon was observed with a variety of nonpolar (oily) substances, including *n*-alkanes, 1-alkenes, 1-alcohols, triglycerides, and their mixtures.[1−4] Furthermore, we observed this phenomenon with substances that do not create self-shaping drops (when used as single components in the oily drops) after mixing them with a moderate amount, above ca. 15 vol %, of another substance, which produces self-shaping droplets upon cooling.[4] The evolution sequence, shown in Figure S1, is common for all tested emulsions. However, different stages of this sequence could be reached in the moment of drop freezing, depending mainly on the specific surfactant−oil combination, the initial drop size, and the rate of emulsion cooling. Also, for small initial droplets with diameter approaching that of the final rods and fibers, the evolution processes are kinetically faster (under otherwise equivalent conditions) and the process of drop flattening may merge with the elongation to rods and fibers. Depending on the specific oil−surfactant couple used, spontaneous transformations were observed to start at a temperature that is a few degrees above, just around, or a few degrees below the bulk melting temperature of the oily phase.[2]

This "self-shaping" phenomenon is of interest for several reasons. On the one hand, it provides a new, highly efficient method for producing micrometer-sized particles with complex regular shapes. These particles could be polymerized, thus producing regular-shaped polymeric microparticles.[5] On the other hand, these systems serve as a new type of versatile toolbox for studying minimal-in-composition systems, which show complex morphogenesis transformations, thus providing insight into the mechanisms generating structure and shape in nature.[2,6] In addition, a new low-temperature method for self-emulsification[7,8] was discovered for some of these systems,

Received: August 15, 2018
Revised: March 27, 2019
Published: March 29, 2019

DOI: 10.1021/acs.langmuir.8b02771
Langmuir 2019, 35, 5484−5495

which is mechanistically based on the drop self-shaping phenomenon and is applicable to temperature-sensitive compounds such as some medical drugs, food supplements, and flavors.

The "self-shaping" phenomenon is far from trivial because it involves a spontaneous increase of the drop surface area with related increase of the system interfacial energy. The drop deformation occurs against the capillary pressure, which acts to preserve the spherical shape of the drops. To explain this nontrivial phenomenon, in our original studies,[1−3] we proposed a mechanism that includes the formation of molecular multilayers of plastic rotator phase,[9−12] templated by the frozen surfactant adsorption layer (see Supporting Information Figure S1b). Indeed, such plastic rotator phases were detected in cooled alkane droplets by X-ray diffraction in earlier studies.[13−15] In our mechanism, the formed multilayer of plastic rotator phase counteracts the finite interfacial tension of the drop surface (of the order of several to 10 mN/m) due to its significant mechanical strength (viz., to its inherent plastoelastic nature). We estimated theoretically the thickness of the rotator phase by making a balance between the bending energy of a plastic surface sheet and the surface energy of the deforming drops.[1] From this estimate, we calculated that the thickness of the rotator phase should be of the order of 15−300 nm.[1,2,16]

An alternative explanation of the same phenomenon was proposed independently by Guttman et al.[17−19] These authors assumed that the interfacial tension of the cooled emulsion drops approaches zero, and therefore the observed drop-shape transformations could be effectuated by the mechanical strength of the surfactant adsorption monolayer, including intercalated alkane molecules,[18] after its freezing on the drop surface.

However, in our previous study,[3] we measured the temperature dependence of the interfacial tensions of several systems undergoing such drop-shape transitions and our results showed unambiguously that drop self-shaping is not related to ultralow oil−water interfacial tension because the drop-shape transformations typically start at temperatures at which the interfacial tension is in the range of 4−8 mN/m for all systems studied by us.

The two alternative mechanisms inevitably focus on different key factors when analyzing the fine details in the mechanism and the main factors for control of the self-shaping and self-emulsification phenomena. The mechanism proposed by Denkov et al. focuses on the conditions for formation of rotator phases in the oily drops, whereas the mechanism proposed by Guttman et al. focuses on the conditions for obtaining very low oil−water interfacial tension. Thus, without having clarity about the underlying mechanism, it is very difficult to approach in a rational way the key questions at the current stage of understanding—how to control and optimize the phenomena of drop self-shaping and self-emulsification for specific systems and applications.

To clarify the detailed mechanism of the observed drop-shape transformations and to determine the thickness of the surface molecular layers, which are directly involved in these transformations, in the current study, we apply differential scanning calorimetry (DSC) to cooled emulsions. DSC is a powerful and very sensitive technique for quantification of the enthalpies of phase transitions.[20] This method is widely used for characterization and analysis of the phase transitions in polymer, ceramic, organic and inorganic, food and pharmaceutical systems, and even in biological organisms.[20−32] DSC has been used also to study the phase transformations in emulsions.[33−40]

The direct characteristics that can be obtained from a typical DSC experiment on emulsions, consisting of one cooling cycle and a subsequent heating cycle, are the temperatures and enthalpies of freezing and melting transitions, the emulsion type, and the fraction of the dispersed phase/medium that undergoes phase transitions.[33−35] As mentioned above, plastic rotator phases were first detected by X-ray diffraction in cooled emulsions containing alkane droplets, in studies that sometimes involved DSC measurements as well.[13−15] In these studies, the droplets were not observed by optical microscopy and, therefore, it has remained unclear whether drop-shape transformations occurred. DSC studies of similar emulsions were performed also by Gülseren and Coupland.[40] These authors studied emulsions containing much smaller droplets, with submicrometer diameter, and alkanes with longer chain length (when compared to the emulsions studied by us) for which the existence of rotator phases upon cooling had been detected earlier.[41] Therefore, these previous papers do not provide direct answers to the research questions that have motivated our current study.

Here, we combine for the first time systematic DSC measurements on emulsions containing "self-shaping" droplets with observations of the drop transformations by optical microscopy. Thus, we are able to determine the fraction of the drop material undergoing phase transition in the temperature range in which the drop-shape transformations occur. The obtained results show that the drop-shape transformations are caused by the formation of ordered multilayers of alkane molecules, with thickness depending strongly on the specific alkane−surfactant combination.

EXPERIMENTAL SECTION

Materials. As dispersed phase, we use two linear *n*-alkanes: hexadecane ($C_{16}H_{34}$) and dodecane ($C_{12}H_{26}$), both with purity of 99%, purchased from Sigma-Aldrich. Detailed information on the physical properties of these alkanes is presented in Supporting Information Table S1. Hexadecane was purified from possible surface-active contaminations by passing it through a glass column filled with Florisil Adsorbent. Very similar results were obtained with purified and nonpurified hexadecanes. Therefore, dodecane was used as received.

For emulsion stabilization, we used the following series of water-soluble nonionic surfactants (in parentheses, their trade name): polyoxyethylene alkyl ethers $C_{16}EO_{20}$ (Brij 58), $C_{16}EO_{10}$ (Brij C10), and $C_{16\text{-}18}EO_{50}$ (Lutensol AT50), and polyoxyethylene sorbitan monoalkylates $C_{12}SorbEO_{23}$ (Tween 20) and $C_{16}SorbEO_{20}$ (Tween 40). All surfactants, except Lutensol AT50 (product of BASF), were purchased from Sigma-Aldrich and were used without further purification. Information on the surfactant properties is presented in Supporting Information Table S2.

All aqueous solutions were prepared with deionized water with resistivity >18 MΩ·cm, purified by Elix 3 module (Millipore). The surfactant concentration was 1.5 wt % in all systems studied, emulsion and surfactant solutions, except for Brij C10 (0.75 wt %), always being well above the critical micellar concentration (CMC) of these surfactants.

Methods. *Emulsion Preparation.* All emulsions were prepared by membrane emulsification in which drops with relatively narrow size distribution are generated.[42−45] The polydispersity index, defined as $\sigma = d_{V84}/d_{V50}$,[46] was 1.14 ± 0.04 for all studied emulsions. We used a laboratory Microkit membrane emulsification module from Shirasu Porous Glass Technology (SPG, Miyazaki, Japan), working with tubular glass membranes of outer diameter 10 mm and working area

DOI: 10.1021/acs.langmuir.8b02771
Langmuir 2019, 35, 5484−5495

of approximately 3 cm^2. The nonpolar (oily) phase was emulsified by passing it through the membrane pores under pressure, into the continuous phase (aqueous surfactant solution). Membranes with mean pore diameters of 1, 2, 3, and 10 μm were used to prepare emulsions with different mean drop diameters. Typically, drops with diameter around 3 times higher than the pore diameter are produced by this method.[44]

DSC Experiments. All DSC experiments were performed on Discovery DSC 250 apparatus (TA Instruments). A sample of the studied emulsion (oil weight fraction, Φ, between 0.3 and 10%) was weighted and placed into a DSC pan (Tzero pan, TA Instruments). Hermetic lid and Tzero sample press (Tzero hermetic lid, TA Instruments) were used to seal the DSC pan before measurements. The samples were cooled and heated at a fixed rate. Based on the results from preliminary experiments, this rate was fixed at 0.5 °C/min in all measurements used to determine the thickness of the multilayers. The reason to choose this rate is that the enthalpy peaks are sufficiently large while the cooling is still sufficiently slow to allow extensive drop shape evolution before the final drop crystallization. The DSC curves upon both cooling and heating were recorded. We performed one cooling and one heating cycle only because of the possible drop−drop coalescence during the heating process. For all studied systems, at least three independent samples were tested (usually between 5 and 10) to obtain sufficient experimental data for statistical analysis and for checking the reproducibility of the final results.

The integration of the DSC curves was performed using the built-in functions of the TRIOS data analysis software (TA Instruments). No baseline subtraction or any other data manipulation was made to determine the peak areas in the thermograms. The horizontal dashed lines drawn in the thermograms, as shown in the figures throughout the paper, are used as guides to the eye only. To allow direct comparison between the various thermograms, in all figures, the thermograms are shifted in vertical direction so that the baseline value is set at zero, and the y-axis is rescaled so that the total peak area corresponds to the total bulk melting enthalpy of the oil contained in the emulsion sample (as determined upon heating). All of these changes affect the visual representation of the DSC data in the figures only—they do not affect in any way the peak area ratios determined by the built-in TRIOS data analysis software of TA Instruments.

Optical Observation in a Capillary. For microscope observations[1−4] of the self-shaping drops, a specimen of the studied emulsion was placed in a rectangular glass capillary of length 50 mm, width 1 mm, and height 0.1 mm. This capillary was enclosed within a custom-made metal-cooling chamber, with optical windows for microscope observation (see Supporting Information Figure S2). The chamber temperature was controlled by cryo-thermostat (JULABO CF30, Cryo-Compact Circulator). The temperature in the sample during the experiment was measured using a calibrated thermocouple probe with an accuracy of ±0.2 °C. The thermoprobe was inserted in one of the orifices of the aluminum thermostating chamber and mounted at a position where a capillary with the emulsion sample would be normally placed for microscope observations. In the neighboring orifices, the actual capillaries with the emulsion samples were placed. The correct measurement of the temperature was ensured by calibrating the thermocouple with a precise mercury thermometer in the range of temperatures measured. After freezing the oily drops, we heated them up until the melting process was observed. We always observe the melting process at temperatures very close, within ±0.2 °C, to the reported melting temperature of the bulk oil, T_m (see Supporting Information Table S1). The rate of emulsion cooling during these optical observations was the same as in the DSC experiments with the same emulsion, thus allowing comparison of the obtained DSC thermograms with the drop shape transformations.

All optical observations were performed with AxioImager.M2m microscope (Zeiss, Germany). We used transmitted, cross-polarized white light, with included λ-compensator plate, situated after the sample and before the analyzer, at 45° with respect to both the analyzer and the polarizer. Under these conditions, the liquid background and the fluid objects have typical magenta color, whereas the frozen birefringent areas appear brighter and may have intense colors.[47,48] We used transmitted light when taking images for the determination of drop-size distribution. Long-focus objectives ×20, ×50, and ×100 were used.

We note that although the oil weight fraction in the studied emulsions is relatively low, the emulsion droplets are able to cream upward in the capillary, under the action of buoyancy. Therefore, the microscopy images presented throughout the paper show a relatively dense monolayer of droplets that creamed from the entire emulsion layer, thus forming a layer with an increased local concentration of the drops.

Optical Observation in a DSC Pan. To check for the actual behavior of the studied emulsion droplets during cooling and heating in the DSC experiments, we performed additional optical observations of emulsion samples, placed in a DSC pan. These experiments were performed as follows: two open DSC pans, containing equivalent emulsion samples, were placed in a metal-cooling chamber, connected to a thermostat. One of the pans was used for optical observations in white reflected light, while in the other pan, we inserted a thermocouple probe to measure its temperature in the course of the experiment (see Supporting Information Figure S3). We performed cooling and heating cycles, at a rate of 0.5 °C/min, similar to those in the actual DSC experiments and in the observations with glass capillaries. We observed the same drop-shape transformations at the same temperatures in both experimental setups (with DSC pans and with optical capillaries). However, the images from the observations in reflected light with DSC pans are not as clear as those obtained with the glass capillaries because the optical system is much superior in the latter experiment. Therefore, we use images from the experiments with glass capillaries to illustrate the observed drop-shape transformations.

Based on the fact that we observe the same drop-shape transformations in both types of experiment (with optical capillaries and with open DSC pans), we accept that the same transformations occur in the closed pans during the actual DSC experiments, which are performed under the same conditions—same temperature range, same scan rate, etc.

Determination of the Drop-Size Distribution in Emulsions. The drop-size distribution in the studied emulsions was determined from microscope images. Drop diameters were measured using the Image Analysis Module of Axio Vision Software. More than 10 000 drops were measured in each sample, and the mean volume-surface diameter $d_{32} = \sum_i N_i d_i^3 / \sum_i N_i d_i^2$ was determined (N_i is the number of drops with diameter d_i). We note that the mean drop size, d_{32}, appears in the estimates of the thickness of the layer of plastic rotator phase, h_{PL}, approximately as $1/d_{32}$, because we determine h_{PL} by comparing the ratio of the peak related to the formation of rotator phase at the drop surface (proportional to d^2) and the peak related to the freezing of the entire drop content (proportional to d^3). Therefore, the final result depends on the specific surface area of the drops, which is, by definition, proportional to $1/d_{32}$. As we measure d_{32} of the initial drops before starting the cooling−heating cycle in the DSC experiments or optical observations, we use hereafter the notation $d_{ini} = d_{32}$ of the initial drops, determined as explained above.

Illustrative histograms of the drop-size distributions by number and volume are presented in Supporting Information Figure S4 for emulsions of hexadecane, stabilized by $C_{16}EO_{20}$ and $C_{16}SorbEO_{20}$ surfactants. From such histograms, by demonstrating the narrow size distribution of the produced emulsions, we can estimate that the error introduced in the layer thickness by the inaccuracy of the measured d_{ini} is around 1% for the 9.5 and 33 μm drops and around 3.5% for the smallest drops studied.

RESULTS AND DISCUSSION

In this section, we present our results from the DSC measurements and connect them to the drop-shape transformations, observed by optical microscopy. Using the ratios between the areas of the enthalpy peaks in the DSC thermograms, we determine the fraction of the intermediate

DOI: 10.1021/acs.langmuir.8b02771
Langmuir 2019, 35, 5484−5495

plastic rotator phase, formed in the course of emulsion cooling, prior to the complete freezing of the oily drops.

In the discussion below, we use the classification of the oil−surfactant systems, introduced in our previous study, ref 2. We classified the various surfactants into four distinct groups, depending on the onset temperature of drop transformation, T_d, compared to the melting temperature of the bulk oil, T_m. Briefly, the surfactants that do not induce drop-shape transformations upon cooling belong to group D. These are surfactants with too short hydrophobic tails and/or with very large head groups. Therefore, their adsorption layers do not freeze at the surface of the cooled drop before the complete oil freezing inside the drops. As a result, the adsorption layers of these surfactants are unable to trigger the formation of plastic rotator phase at the drop surface for the respective oil. In groups A to C, we place surfactants that induce drop-shape transformations upon cooling: surfactants in group A are those for which $T_d > T_m$; group B contains surfactants for which $T_d \approx T_m$; and group C contains surfactants for which $T_d < T_m$; for more details, see ref 2 and Supporting Information Table S3.

Below we show and discuss separately the experimental results obtained with representative oil−surfactant pairs from these groups.

In Figure 1, we present the DSC thermogram, obtained with hexadecane (C_{16}) drops for which $T_m \approx 18$ °C, dispersed in $C_{16\text{-}18}EO_{50}$ surfactant solution. For this oil−surfactant pair, the surfactant falls into group D because it has a very voluminous head group of 50 ethoxy units and it does not induce drop-shape transformations upon cooling.[2] As seen from the DSC curve, we observe one main peak with Gaussian shape, centered around 6 °C, and two small peaks around 15 °C.

In the microscope observations in capillary, we saw freezing of a very small fraction of the oily droplets to start in the temperature range of 9.3−7.5 °C, but the main fraction of the oil drops were seen to freeze around 6 °C (see Figure 1b−d). These optical observations can be directly related to the peaks in the measured DSC thermogram. As seen in Figure 1, the DSC signal starts to deviate slightly from the baseline at a temperature of 9−10 °C, while the main peak, caused by the bulk freezing of the emulsion drops, is observed at a temperature around 6 °C. The Gaussian shape of the main DSC peak is expected; although the drops are relatively monodisperse, the nucleation in the individual drops occurs at slightly different moments, resulting in a drop freezing within a certain temperature range, rather than at fixed temperature.[32,33]

The observations in a glass capillary did not show any sign of drop freezing at 15 °C. However, when we performed optical observations in a DSC pan, we observed multiple oil lenses floating on the surface of this particular emulsion sample, as well as some very big emulsion drops (Figure 1e−g). Both the oil lenses on the emulsion surface and the large emulsion drops were freezing at a temperature around 15 °C. Thus, we conclude from these observations that the DSC peaks, observed around 15 °C, are due to crystallization of C_{16} in the large oil lenses and the large oil drops, at temperatures slightly lower than T_m, as a result of the moderate undercooling (by around 3 °C) of the oil in these large entities.

Similar DSC results and explanations were reported by Shinohara and co-authors.[15] They present DSC data, obtained at a cooling rate of 2 °C/min, for C_{16} drops with initial diameter, d_{ini} = 32.6 ± 3.2 μm, stabilized by 1 wt % aqueous solution of Tween 20 surfactant ($C_{12}SorbEO_{20}$). This surfactant also belongs to group D, according to our classification, because its C_{12} tail is by four carbon atoms shorter than the alkane chain length. Therefore, this surfactant does not induce drop-shape transformations upon cooling of hexadecane emulsions, as confirmed in our experiments. For this system, Shinohara and co-authors observed two exothermic peaks, one at 14.5 °C interpreted as bulk C_{16} crystallization and a second broad peak with a maximum around 5.5 °C, corresponding to crystallization of the alkane in the oily drops (see Figure 2 in ref 15). We also performed DSC and microscopy experiments with the same system—C_{16} drops, stabilized by $C_{12}SorbEO_{20}$ surfactant. The DSC results were very similar to those reported in ref 15. The optical observations of the emulsions in the DSC pan showed that oil lenses were formed on top of this sample as well (see Supporting Information Figure S5). The peak around 15 °C is associated with the freezing of these lenses.

We studied several other oil−surfactant pairs from group D and observed the same phenomena with all of them. This type

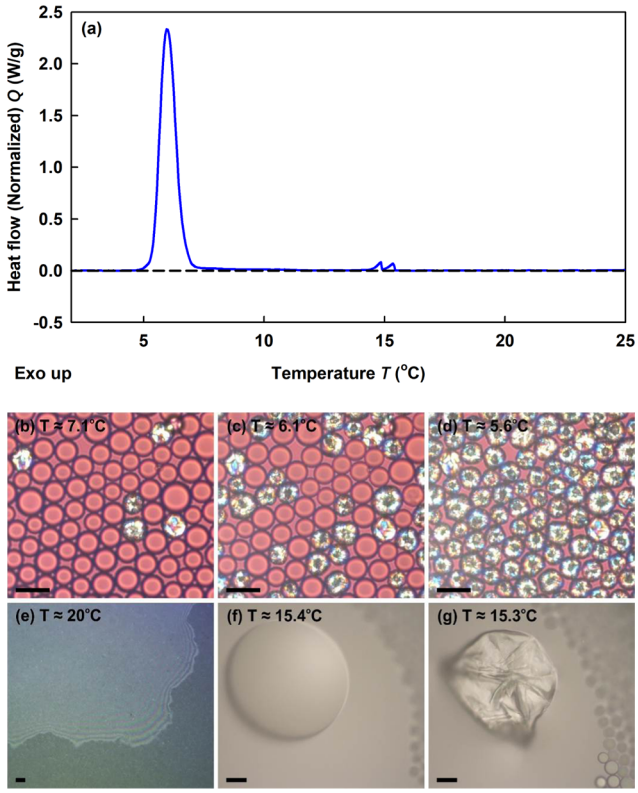

Figure 1. DSC thermogram and microscopy images for C_{16} drops with initial drop size, $d_{ini} \approx 10$ μm, stabilized by $C_{16\text{-}18}EO_{50}$ surfactant (group D). (a) DSC thermogram upon cooling; (b−d) Microscopy images in transmitted polarized light, showing the process of drop freezing upon cooling. The cooling experiment is performed in glass capillary. (b) The first freezing process is observed at temperature 9.3 °C; however, as seen in this picture, only a very small fraction of the drops have frozen down to 7.1 °C. (c, d) The main freezing process is observed between 6.5 and 5.6 °C. (e, f) Cooling experiment of the same sample, contained in a DSC pan. The drops are observed in reflected white light. The small peaks, observed in the thermogram around 15 °C are due to the freezing of the oil lenses and some large drops, formed after drop−drop coalescence. (e) Oil lenses are observed at the top of the sample, placed in a DSC pan. (f) Fluid big drop. (g) The drop freezes at a temperature of 15.3 °C. All experiments (both DSC and optical observations) are performed at 0.5 °C/min cooling rate. The scale bar is 20 μm.

DOI: 10.1021/acs.langmuir.8b02771
Langmuir 2019, 35, 5484−5495

of behavior is caused by the fact that the surfactants in these emulsions do not form densely packed adsorption layers, due to their relatively short hydrophobic tail and/or relatively large hydrophilic head. As a result, the surfactants do not stabilize well the respective emulsions and oil lenses emerge on the emulsion surface and/or drop−drop coalescence is observed.[49] The formed larger entities (oil lenses/drops) freeze at temperatures around and slightly below T_m, while the main fraction of the drops freeze at a much lower temperature, without undergoing drop-shape transformations. The formation of oil lenses and/or huge emulsion drops was not observed for any of the other tested systems from groups A to C.

Group B: Surfactants which Induce Drop Self-Shaping at $T_d \approx T_m$. The data interpretation for surfactants inducing drop-shape transformations is most straightforward for the surfactants from group B. Therefore, we present first the results for an emulsion that is representative for this type of systems: C_{16} drops with $d_{ini} \approx 9.5 \pm 0.1$ μm, stabilized by $C_{16}SorbEO_{20}$. The respective DSC curve and microscopy images are shown in Figure 2.

Before discussing the results for this system, we should emphasize that we do not observe any measurable peaks in the cooling DSC thermograms of the surfactant solution of $C_{16}SorbEO_{20}$ without dispersed oil (see Supporting Information Figure S6). No peaks are observed in the temperature interval 0−30 °C also for emulsions containing drops of shorter-chain alkanes (e.g., C_{12}), stabilized by a long-chain surfactant in which the oil drops freeze at much lower temperatures (see Supporting Information Figures S7). Thus, we can conclude that all peaks observed in the thermograms presented below are due entirely to the enthalpy release upon ordering of the alkane and surfactant molecules in the emulsion drops, viz., these peaks do not contain any enthalpy contribution generated by changes in the surfactant aggregates (micelles) in the aqueous phase.

The cooling thermogram of C_{16} drops dispersed in $C_{16}SorbEO_{20}$ solution shows four major exothermic peaks (Figure 2a). The first peak starts sharply at 15.2 ± 0.2 °C (data from four independent measurements); for this particular sample, the peak starts at 15.4 °C and returns back to the baseline at 14.8 °C. The second peak starts from around 14 °C and continues down to 11 °C, where the third major peak starts to develop. The third and fourth peaks largely overlap and return back to the baseline at 5 °C. The total area of these peaks corresponds to the total enthalpy of complete freezing of the dispersed alkane. The freezing of all drops at the lowest temperature is confirmed by optical observations. Therefore, by comparing the measured enthalpy in the emulsion experiments to the enthalpy of freezing of pure hexadecane (≈ 235 J/g),[9] we can calculate the actual oil weight fraction, Φ, in the emulsion studied

$$\Phi = \frac{H_{m,emulsion}}{H_{m,bulk\ oil}} \quad (1)$$

We note that we do not use the calculated oil weight fraction anywhere in the data interpretation. We always use the ratio between the enthalpy peaks measured in specific temperature range upon cooling and the total enthalpy of drop melting measured upon heating of the same sample. Typical emulsion heating thermograms are presented as Figure S8 in the Supporting Information.

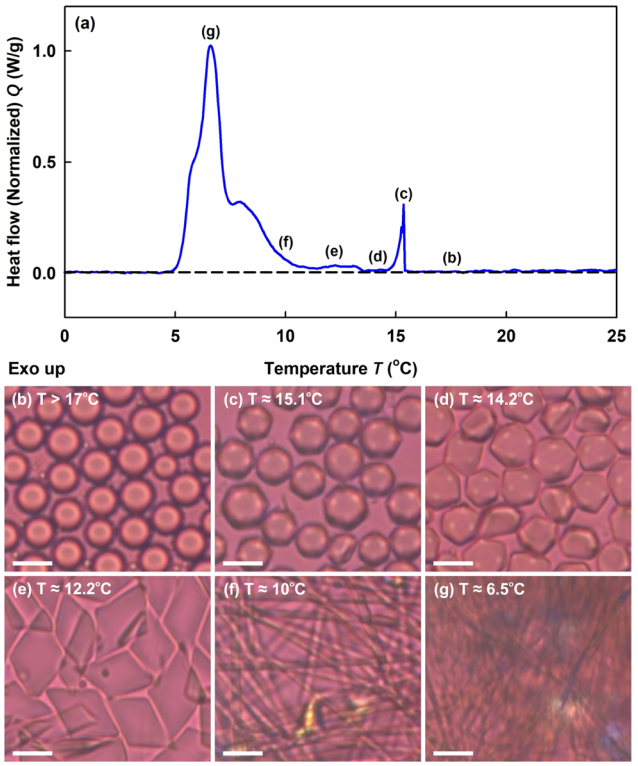

Figure 2. DSC thermogram and microscopy images for C_{16} drops with $d_{ini} \approx 9.5 \pm 0.1$ μm, stabilized by $C_{16}SorbEO_{20}$ surfactant (group B). (a) DSC thermogram, obtained at 0.5 °C/min cooling rate; (b−g) Microscopy images showing the different stages of the drop-shape evolution upon cooling; cooling rate, 0.5 °C/min. (b) All emulsion drops are spherical at temperatures above 17 °C. (c) Drop-shape transformations start around 15.2 ± 0.2 °C (data from four independent measurements); for this particular sample, the peak starts at 15.4 °C. At this temperature, the DSC curve starts to deviate from the baseline. (d) At temperature around 14.2 °C, flattened polyhedrons are formed. (e) The decrease of the temperature leads to further evolution in drop shape. At temperature around 12.2 °C, drops have evolved up to the stage of tetragonal platelets. (f) Some rare drops were observed to freeze at 11 ≤ T ≤ 12 °C, while most of the drops elongate into long fibers. (g) The thin elongated fibers freeze (crystallize) completely at $T \approx 6.5$ °C. The scale bar is 10 μm.

The two overlapping peaks at the lowest temperature in Figure 2a correspond to the complete freezing of the deformed hexadecane drops into crystalline phase (cf. Figure 2f,g). Note that the temperature of the rotator-to-crystal phase transition differs significantly from the temperature of the liquid-to-crystal phase transition only for the alkanes with thermodynamically stable (or metastable) bulk rotator phase, like that in the interior of the mixed alkane drops.[12,50] The rotator phase in bulk hexadecane is thermodynamically classified as "transient" and it is very short leaving.[12] Therefore, in Figure 2a, we do not observe a separate rotator-to-crystal phase transition from the liquid-to-crystal phase transition inside the interior of the hexadecane drops—the first formation of true crystal phase in the drops acts as a nucleus for the complete crystallization of the hexadecane drop interior into the final, truly crystalline form.

On the other hand, we do not observe any freezing (crystallization) of the drops in these emulsions down to 12 °C—neither in the capillary experiments nor in the DSC pan experiments. Therefore, the peaks observed above 12 °C are related entirely to enthalpy released in the process of molecular

DOI: 10.1021/acs.langmuir.8b02771
Langmuir 2019, 35, 5484−5495

rearrangement of the hexadecane in the nonfrozen oil drops (with a possible contribution from the freezing surfactant adsorption layer). Let us relate now these peaks to the observed shape transformations in the deforming drops (Figure 2).

The highest-temperature peak appears at the temperature at which we observe the initial drop-shape changes. As seen in Figure 2c, at a temperature of 15.1 °C, all drops have evolved into regular polyhedrons. Thus, we conclude that the first peak is related to the process of polyhedron formation. The second peak corresponds to the next stages of the drop-shape evolution, in which the polyhedrons flatten and hexagonal platelets are formed (cf. Figure 2d). Upon further cooling, the drops transform into tetragonal platelets. The subsequent stage is elongation of the tetragons and their transformation into thin fibers. However, some drops freeze in the shape of elongated prisms, before transforming into fibers (cf. Figure 2f).

The enthalpy, measured from the beginning of the drop-shape transformations up to the formation of tetragonal platelets at a temperature of 12.2 °C, is around 3.8 ± 0.6% from the total enthalpy measured in the whole DSC experiment (average from four independent measurements; see also Supporting Information Figures S9 and S10). This means that ≈3.8% of the total enthalpy has been released along the transition from isotropic liquid phase into a phase with higher order, before any freezing of the oily drops is observed. From the optical observations, we can calculate the average geometric parameters of the platelets formed at this temperature (see Figure 3a). The side lengths of the platelets are 12.5

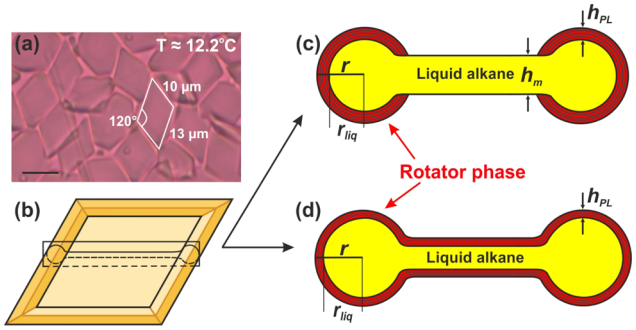

Figure 3. Calculation of the rotator phase thickness for tetragonal platelets (group B). (a) Microscopy image of fluid tetragonal platelets obtained upon cooling of C_{16} emulsion sample stabilized by $C_{16}SorbEO_{20}$ surfactant. The initial drop size is $d_{ini} \approx 9.5$ μm; drops are cooled at 0.5 °C/min. The scale bar is 10 μm. (b) Sketch of a fluid platelet. (c, d) Sketches of two alternative models used to estimate the thickness of the rotator phase, formed at the platelet surface: (c) model I: Geometrical model, in which it is assumed that the rotator phase is formed only at the platelet periphery (in the regions of high interfacial curvature) while the alkane in the inner part of the drop is in the liquid state; (d) model II: Geometrical model using the assumption that a homogeneous layer of rotator phase is formed over the entire surface of the deformed drop. See text for more details.

± 2 μm, while their obtuse angle is 120 ± 8°. The three-dimensional shape of the platelets is shown schematically in Figure 3b. For the following estimate, this shape can be approximated in the following way: the periphery of the platelet is approximated with a cylinder of radius r, while the volume of the inner part of the platelet is represented as a plane-parallel platelet (Figure 3c,d). As the drops change their shape at a fixed drop volume, the average thickness of this central part of the tetragonal platelets can be calculated from the volume conservation principle (see Supporting Information Section 1 for more details). Thus, from the measured geometrical parameters and the enthalpy of the tetragonal platelets, we can estimate the thickness of the new phase, formed at the drop surface in the process of drop-shape transformation. We have made these estimates using two different assumptions to capture the upper and lower boundaries of the rotator phase thickness.

As an upper limit for the estimate of the thickness of the formed rotator phase (model I), we assume that the latter is formed only at the platelet periphery (along the curved perimeter edges), while no rotator phase is formed on the flat surface in the central part of the platelet (Figure 3c). This assumption is supported by the symmetric drop breakage observed upon cooling of such platelets;[7,8] indeed, if the rotator phase was formed in the central region, it would stabilize the particles against puncturing of the platelet in this central region. Under this assumption, the volume of the formed rotator phase, V_{PL}, may be estimated as explained in Supporting Information Section 2a. In these estimates, important parameters are the thickness of the plastic (rotator) phase, h_{PL}, and the thickness of the plane-parallel body in the particle center, h_m, which may vary in the general case between $h_m \to 0$ (very thin central part) and $h_m \approx 2r$ (flat platelet) in this consideration (see Figure 3c). The fraction of the formed rotator phase (compared to the total drop volume) is equal to the ratio of the enthalpy released down to the temperature at which the deformed drop is analyzed and the total enthalpy of complete drop freezing, corrected by a constant, k

$$\frac{V_{PL}}{V_{total}} = \frac{kH_{PL,\text{down to } T=12.2\ ^\circ C}}{H_{total}} \approx 0.038k \qquad (2)$$

where 0.038 = 3.8% is the measured fraction of the total enthalpy. The parameter k takes into account the fact that the enthalpy of formation of the rotator phase (per molecule) is a fraction of the total enthalpy of complete freezing of the molecules included in the rotator phase. This parameter represents the ratio of the enthalpy of formation of the crystalline phase to the enthalpy of formation of the rotator phase, in both cases starting from liquid phase, for the same alkane amount. From the literature data,[9] we know that the enthalpy of formation of the rotator phase is around 80% of the total enthalpy of complete oil freezing for pentadecane and heptadecane. Therefore, we assume $k \approx 1/0.8 = 1.25$ in our estimates. The total volume, $V_{total} = \pi d_{ini}^3/6$, is the volume of the initial drop. Substituting the experimental parameters in eq 2, we can estimate the fraction of the rotator phase formed. As average values from our measurements we take $d_{ini} = 9.5 \pm 0.1$ μm. The value of h_m may vary significantly during the cooling process. To estimate the thickness of h_{PL}, we assumed a certain ratio for the thickness of the middle platelet over the cylinder radius, h_m/r, and checked which value of the thickness of the rotator phase would satisfy the equation for the rotator phase volume (eq S10 in the Supporting Information), while the values of h_m and r satisfy simultaneously equation for the total platelet volume (eq S6 in the Supporting information). In this way, we determined the possible variation of h_{PL}, which satisfies all experimentally determined quantities, in the range of reasonable values of the ratio $0 < h_m/r \leq 2$. From these

DOI: 10.1021/acs.langmuir.8b02771
Langmuir 2019, 35, 5484−5495

calculations, we found that the h_m varies in the range of 0.4 μm for $h_m = 0.2r$ to 3.2 μm for $h_m = 1.9r$. Respectively, the values of r vary between 2 and 1.7 μm. The mean value of h_m for the whole range is 1.8 ± 1.2 μm, while for r, it is 1.85 ± 0.3 μm. Performing these calculations, we found that the thickness of the plastic phase falls in the range of 49 ± 5 nm for $h_m = 0.2r$ to 70 ± 5 nm for $h_m = 1.9r$. The standard deviations are calculated by making calculations for more than 15 deformed drops using each of the above assumptions. Thus, we see that the most probable value of h_{PL} is around 55 ± 15 nm, where the standard deviation accounts also for the uncertainty in the values of h_m. Further variations of h_m in the entire range between 0 and 2r do not change this main result of the calculations and the related conclusions. The lamellar spacing for hexadecane molecules in pseudohexagonal rotator phase is 2.26 nm,[13] which means that the estimated thickness corresponds to a multilayer of ≈24 ± 6 parallel layers of ordered hexadecane molecules, corresponding to the range between 18 and 30 ordered alkane layers.

To estimate the lower limit of the rotator phase thickness from the measured DSC peak areas, we adopted an alternative assumption (model II), namely, that a homogeneous layer of rotator phase is formed over the whole surface of the platelet (Figure 3d). We should note that the available experimental results do not support this assumption. Nevertheless, it could be used to find the minimal possible thickness of the rotator phase in these emulsions. Under this assumption, $V_{PL}=Sh_{PL}$, where S is the surface area of the platelet. The total volume of the rotator phase and the related thickness h_{PL} in this model are estimated as explained in Supporting Information Section 2b. Using the same assumptions as in the previous model, with the same r values, which vary between 1.7 and 2 μm, we estimated the thickness of the rotator phase to fall in the range of 40 ± 7 nm for $h_m = 0.2r$ to 51 ± 6 nm for $h_m = 1.9r$. Thus, we see that the most probable value of h_{PL} in this model is around 45 ± 13 nm.

Similar, though less precise estimate could be made for the thickness of the rotator phase, formed at the very early stage of polyhedrons formation (Figure 2c). For this estimate, we assume that a homogeneous rotator phase is formed on the entire surface of the polyhedrons and the respective enthalpy is reflected only in the first peak, observed at around 15 °C. Thus, we estimated the thickness of the rotator phase to be ≈36 nm for assumed icosahedral shape of the deformed drop and ≈32 nm for assumed octahedral drops. The latter, very close values show that this estimate is weakly affected by the assumed specific shape of the polyhedrons. Furthermore, the agreement in the values for h_{PL} with the estimate performed above for the platelets shows that all of these estimates are robust with respect to specific details in the assumptions made.

DSC and microscopy experiments were performed also with smaller emulsion drops, d_{ini} ≈ 3 μm, from the same emulsion system: C_{16} drops, dispersed in $C_{16}SorbEO_{20}$ surfactant solution. The DSC curve and the respective microscopy images are shown in Figure 4. The main observed difference between the two latter systems (9.5 μm vs 3 μm drops) was in the kinetics of the drop-shape evolution, as explained in ref 2. The smaller drops evolved much faster, viz., for shorter time under otherwise equivalent conditions, up to the last stages of the evolutionary scheme, forming triangular platelets and long thin fibers (Figure 4d–f).

The DSC curve, obtained with these smaller drops, starts to deviate sharply from the baseline at a temperature of 15 ± 0.3 °C (data from 10 independent measurements); for this particular sample, the deviation starts at 14.7 °C and the maximum of the first peak is at 14.6 °C (cf. Figure 4a,d). The microscopy observations showed that the drops started to deform around 17 °C, where the small deviation from the baseline does not allow us to measure reliably the initial enthalpy effects (see Figure 4c). The first observed peak at ≈15 °C corresponds to the drop-shape transformation from regular polyhedrons into long rods and trigonal platelets (Figure 4d). These trigonal platelets freeze at a temperature of around 13.5 °C (Figure 4e), while the rodlike droplets elongate further into thin fibers and freeze completely at a much lower temperature, around 5.5 °C (Figure 4g).

From these results, we can calculate the thickness of the rotator phase in the thin fibers like those shown in Figure 4d. By integrating the DSC peak down to 13.8 °C, we calculated that the enthalpy of formation of the fibers with length of around 15.2 ± 2.3 μm is around 2.7 ± 0.8% of the total enthalpy of all peaks (data from 10 independent experiments).

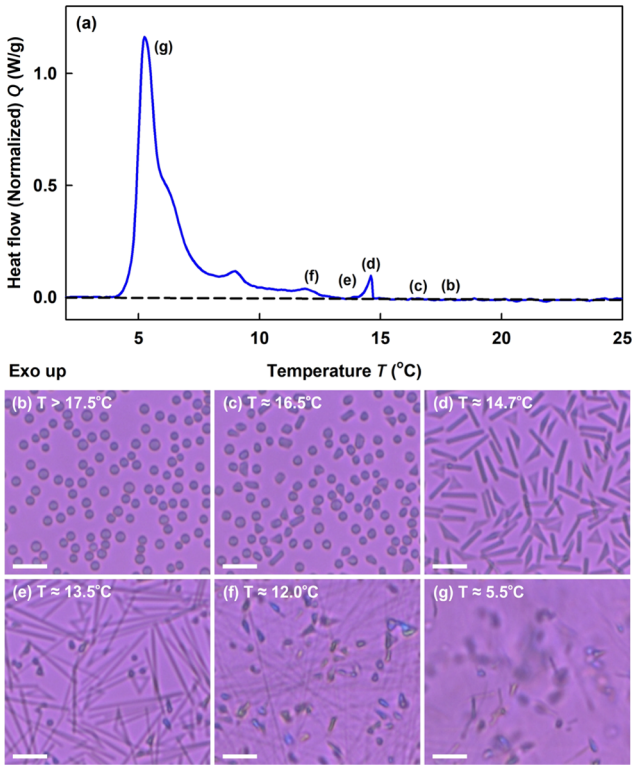

Figure 4. DSC thermogram and microscopy images for C_{16} drops, d_{ini} ≈ 3 μm, stabilized by $C_{16}SorbEO_{20}$ surfactant (group B). (a) DSC thermogram, obtained at 0.5 °C/min cooling rate. (b–g) Microscopy images showing the different stages of the drop-shape evolution upon cooling; cooling rate, 0.5 °C/min. (b) All emulsion drops are spherical at temperatures above 17.5 °C. (c) Significant drop-shape transformations start in the range of 17–15 °C. The initial weak deviation of the DSC curve from the baseline is followed by a sharp deviation at 15 ± 0.3 °C (data from 10 independent measurements); for the thermogram presented in the figure, the curve deviates sharply at 14.7 °C. (d) At temperature around 14.7 °C, rod-shaped entities are formed. (e) At temperature around 13.5 °C, the drops evolved into long rods and the first drop freezing is observed. (f) Thin fibers are formed around 12 °C, along with additional drop freezing. (g) All thin fibers freeze at temperature around 5.5 °C drops. The scale bar is 10 μm.

DOI: 10.1021/acs.langmuir.8b02771
Langmuir 2019, 35, 5484–5495

In this case, the ratio of the volume of the rotator phase to the total drop volume can be expressed as

$$\frac{V_{PL}}{V_{total}} = \frac{kH_{PL,down\ to\ T=13.8\ °C}}{H_{total}} \approx 0.027k \quad (3)$$

where the constant $k = 1.25$ has the same meaning and value as in eq 2. To estimate the thickness of the rotator phase formed on the fiber surface, we assume that it is formed along the surface of the whole fiber and has uniform thickness. Thus, we model the fibers as two coaxial cylinders with different radii, the inner cylinder with radius r_{liq} is filled with isotropic liquid oil, while the space between the outer cylinder (with radius r) is occupied by plastic rotator phase (Figure 5).

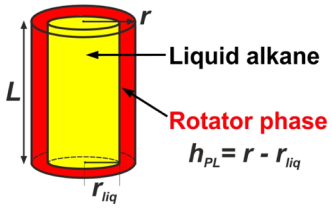

Figure 5. Calculation of the rotator phase thickness for the rodlike fluid drops (groups B and C). Sketch of the geometrical model used for calculation of the rotator phase thickness in rodlike fluid drops. The rotator phase is formed with homogeneous thickness on the drop surface, while the core of the drop contains isotropic liquid (see text for details).

As illustrated in Figure 5, the volume of the liquid phase is $V_{liq} = \pi r_{liq}^2 L$, the volume of the plastic phase is $V_{PL} = \pi L(r^2 - r_{liq}^2)$ and the total volume is $V_{total} = \pi d_{ini}^3/6 \approx \pi r^2 L$, where L is the length of the rodlike particle. In the last equation, we have neglected the volume of the two hemispherical caps at the rod ends because the ratio $r/d_{ini} \ll 1$. Using these relations and the fact that the rods at this moment are around 15 μm long, we calculate the thickness of the rotator phase, $h_{PL} = r - r_{liq}$, to be around 9.4 ± 3 nm, corresponding to a multilayer of around 4 ± 1 molecules thick.

We did not try to determine h_{PL} for the drop shapes in the earlier stages of the drop evolution (shown in Figure 4) because the molecular layers might be distributed non-homogeneously on the drop surface for the more complex drop shapes, and such an estimate would inevitably involve some speculative assumptions.

In conclusion, the experiments performed with C_{16} drops, stabilized by C_{16}SorbEO$_{20}$ surfactant (group B), show unambiguously that the drop-shape transformations in this system are caused by the formation of multilayers of ordered alkane molecules. The thickness of the layers varies between ≈10 nm for the smallest studied drops, which transform into thin fibers, and ≈55 ± 15 nm for the intermediate in size drops, which transform into tetragonal platelets.

Group C: Surfactants Which Induce Drop Self-Shaping at $T_d < T_m$. Similar experiments were performed with hexadecane drops with initial diameter $d_{ini} \approx 2.6$ μm stabilized by C_{16}EO$_{20}$ surfactant. This is a surfactant from group C in our notation because the drop-shape transformations start at $T_d < T_m$ (see Supporting information Table S3). The DSC curve and the respective microscopy images are shown in Figure 6. As expected, the first deviation from the baseline in the DSC signal is observed at ≈10.5 °C when the drop-shape transformations start. The thermogram has two

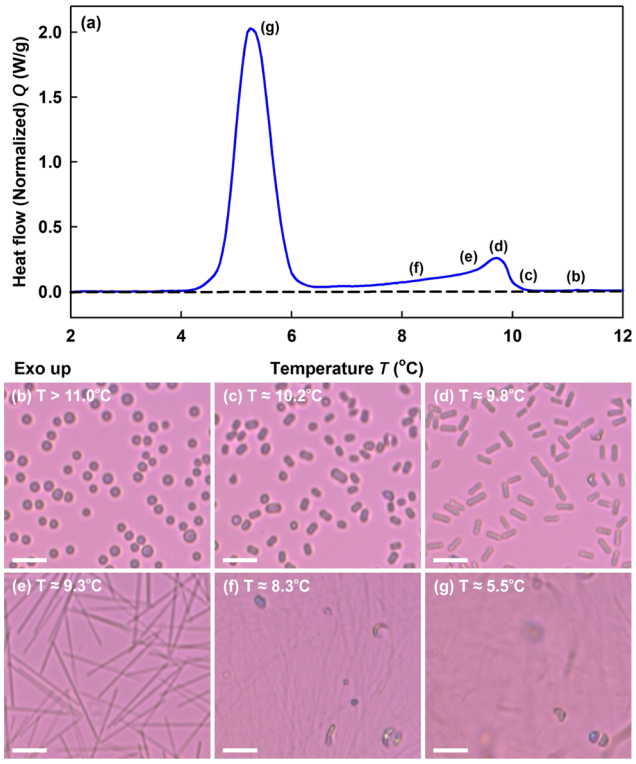

Figure 6. DSC thermogram and microscopy images for C_{16} drops, d_{ini} ≈ 2.6 μm, stabilized by C_{16}EO$_{20}$ surfactant (group C). (a) DSC thermogram, obtained at 0.5 °C/min cooling rate. (b–g) Microscopy images showing the different stages of the drop-shape evolution upon cooling; cooling rate, 0.5 °C/min. (b) All emulsion drops are spherical at temperatures above 11 °C. (c) Drop-shape transformations start around 10.5 °C and drops rapidly evolve into short rods. At this temperature, the DSC curve starts to deviate from the baseline. (d, e) With the decrease of the temperature, the rod length increases, while the diameter decreases. (f) Thin long fibers are formed from the rods. Some colored frozen drops are seen, which had been frozen at higher temperatures, ca. at $T \approx 10$ °C. (g) Freezing of the fibers. At this temperature, the second peak in the DSC thermogram is observed. The scale bar is 10 μm.

exothermic peaks, one broad peak from 10.5 to 6.5 °C and a second peak with higher intensity between 6.5 and 4 °C. From five independent samples, we calculated that the enthalpy of the first peak is around 16.5 ± 1.2%, while the second peak has enthalpy around 83.5% of the total enthalpy. This second peak corresponds to the final freezing of the droplets (see Figure 6g). The Gaussian shape of this peak is expected because all drops that had not been frozen until that temperature had transformed into long fibers with very similar shape and dimensions, and therefore they all freeze at similar temperatures.

The interpretation of the first peak is not straightforward. As seen in Figure 6d, almost all drops have evolved in shape into short rods at $T \approx 9.8$ °C. However, two of the particles in this image had frozen at an earlier stage of their evolution. Statistical analysis over >2500 drops showed that 8 ± 2% of the drops in these emulsions freeze at temperature around 10 °C, while the rest of the dispersed entities evolve into the later stages of the evolutionary scheme and freeze around 5–6 °C. On the other hand, the enthalpy of the first peak (16%) is about two times larger than that originating from the drops frozen at this stage (8% frozen drops). Therefore, we can

DOI: 10.1021/acs.langmuir.8b02771
Langmuir 2019, 35, 5484–5495

conclude that about half of the first peak is due to the enthalpy released around 10 °C in the process of drop deformation without alkane freezing. In other words, about 8% of the enthalpy is due to the formation of ordered multilayers of alkane molecules in a rotator phase, causing the drop-shape transformations.

This data interpretation is supported also by the fact that the first peak in the thermogram is observed throughout a wide temperature range, from 10.5 to 6.5 °C, and the DSC curve returns to its baseline only after the final freezing of all drops (see the punctured black line in Figure 6a). However, an initial freezing of the drops happens around 10 °C only, whereas no further freezing (crystallization) of drops is observed between 10 and 6.5 °C because all drops that had acquired rodlike shape did not freeze down to 5−6 °C (see Figure 6c−f). This means that the DSC signal observed between 10 and 6.5 °C is entirely associated with the drop-shape transformations, observed in this temperature range. From the area of this peak, assuming that the rotator phase is formed as a thin layer over the entire surface of the rod-shaped droplets (same assumption as that shown in Figure 5), we estimated the thickness of the rotator phase as 8 ± 2 nm (viz. 3 ± 1 alkane layers). For this estimate, we used d_{ini} = 2.6 μm and $L \approx 120$ μm. The fiber length was estimated from the diameters of the drops formed after one freeze/thaw cycle in this emulsion system. As explained in ref 7, the diameter of the drops formed after fiber melting via the Rayleigh−Plateau type of instability is around 1.9 times larger than the diameter of the fibers from which they have been formed. As shown in ref 7, the drop diameter after one freeze/thaw cycle in this emulsion is around 600 nm (by number), i.e., these drops are formed from fibers with diameter of ≈315 nm, which corresponds to $L \approx 120$ μm.

Group A: Surfactants Which Induce Drop Self-Shaping at $T_d > T_m$. To complete this study with all different types of surfactant, here we present our DSC and microscopy results for the surfactants that induce drop-shape transformations at $T_d > T_m$, viz., for the surfactants from group A. The studied emulsions contained C_{16} drops with $d_{ini} \approx 33$ μm, stabilized by $C_{16}EO_{10}$ surfactant. In this system, the drop-shape transformations start at ≈23 °C, while the drop freezing is observed predominantly in the range of 14−15 °C. The drops in this system behaved differently from the systems discussed in the previous paragraphs—first, polyhedrons with irregular shape and corrugated surface are formed and several subsequent breakage events are observed upon cooling (see Movie S1). After each breakage event, several smaller drops are formed, while the main fraction of the oil remains in the central ("mother") drop.[8]

Two DSC thermograms, measured independently with this system, are presented in Figure 7a,b. As seen in Movie S1 and in Figure 7d, the drop-shape transformations start well above the temperature at which the process of freezing is observed (≈15 °C). The first drops start to change their shape at a temperature around 22.5 °C, but the massive drop transformations are observed in the temperature range of 22−21 °C. As expected, in the range 21−22 °C, the DSC curve significantly deviates from the baseline well above the noise signal, forming a small but well reproducible and non-negligible peak. This peak was observed with all tested samples (more than three) from this type of emulsion. At temperatures below this peak, we observe continuous exothermic deviation of the DSC curve above the baseline, which reflects the continuous drop-shape transformations in this temperature range (see Movie S1).

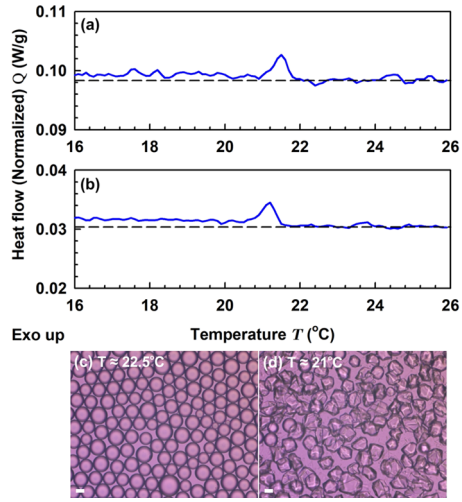

Figure 7. DSC thermogram and microscopy images for C_{16} drops, d_{ini} ≈ 33 μm, stabilized by $C_{16}EO_{10}$ surfactant (group A). (a, b) DSC thermograms, obtained at 0.5 °C/min cooling rate from two independent measurements for the temperature interval between 16 and 26 °C. Note that although the peak observed between 20 and 22 °C is relatively small, it is well reproducible. Furthermore, the curve stays above the baseline value at T < 22 °C, which reflects the continuous drop-shape transformations in this temperature range. (c, d) Microscopy images showing the different stages of the drop-shape evolution upon cooling; cooling rate, 0.5 °C/min. (c) Most of the drops are spherical at temperatures above 22.5 °C (see Movie S1). (d) All of the drops have changed their shape at 21 °C. The thermograms are rescaled only with respect to the oil weight fraction; the baselines have not been shifted to "zero" value.

To estimate the rotator phase thickness in these emulsions, we used two alternative assumptions. The first assumption is that a rotator phase with uniform thickness is formed on the entire drop surface. This assumption allows us to calculate the lower limit of the rotator phase thickness. As the initially formed shapes are irregular, we cannot calculate precisely their surface area. Therefore, to estimate approximately the realistic range of surface areas of these drops, we calculated the surface area of several polyhedrons having the same volume. Assuming that the spherical drop is transformed into regular polyhedron (icosahedron, octahedron, or cube), we found that the surface of the deformed bodies increases by less than 25%, compared to the initial spherical surface. Therefore, the thickness of the rotator phase is bound within the limits $V_{PL}/S_{IN} \geq h_{PL} \geq V_{PL}/1.25S_{IN}$, where S_{IN} is the surface area of the initial spherical drop. Comparing the volume of the rotator phase to the total volume and the areas of the peaks from the thermogram, we obtained that the thickness of the plastic phase is 6.25 nm ≥ h_{PL} ≥ 5.00 nm (two to three layers). In this estimate, we used d_{ini} = 33 μm, k = 1.25, and enthalpy ratio $(H_{PL}/H_{total}) \approx 9.1 \times 10^{-4}$, as measured experimentally.

Alternatively, if we assume that the rotator phase is formed not as a homogeneous layer on the entire surface of the polyhedral entities but on the edges of the polyhedrons only (an assumption that corresponds much better to our explanation[1−4] for the origin of the drop-shape transformation), then we estimated that the rotator phase would be with thickness that is much larger, between ca. 30 and 180 nm, depending on the specific assumptions made. This range

DOI: 10.1021/acs.langmuir.8b02771
Langmuir 2019, 35, 5484−5495

of h_{PL} values was estimated assuming icosahedral shape of the deformed drops and some additional assumptions for the specific shape of the strips of rotator phase, formed along the edges of the icosahedral drop (see Section S3 of the Supporting Information for detailed explanations). Two theoretical models have been tested to make these estimates, and both models gave similar results, as described in Section S3 of the SI. Therefore, for the emulsions stabilized by surfactants from group A, we cannot make a final conclusion about the thickness of the rotator phase until we have additional experimental information about the distribution of the rotator phase on the surface of the polyhedrons. Nevertheless, we conclude that neither of the performed realistic estimates could explain the drop-shape transformations as a result of freezing of the adsorption monolayer only.

Thus, we can conclude from all performed experiments that the enthalpy of the peaks, observed before the complete freezing of the alkane drops, is related to the formation of multilayers of ordered alkane molecules on the drop surface for all systems studied. The thickness of these multilayers depends significantly on the specific surfactant−oil pair. Some of the results indicate that the thickness of the multilayer depends on the size of the deforming droplets as well.

Thickness and Mechanical Strength of the Layers of Rotator Phase. To preserve the observed characteristic curvature with radius $r \approx 1$ μm at the edges of shaped droplets, at a finite interfacial tension γ, we need to overcome the capillary pressure, which would otherwise unfold the shapes into spherical drops with minimal surface energy. The balance of the bending moments created by the interfacial tension and the plastic rotator phase requires that the bending elasticity constant of the plastic phase formed at the surface of the shaped drops should satisfy the relation[1−3]

$$K_B \geq \gamma r^2 \tag{4}$$

where K_B is the bending elasticity constant of the interface (including the multilayers of the rotator phase).

In our original papers,[1−3,16] we estimated the thickness of the layers of rotator phase, which can deform the surface of the oil droplets with an interfacial tension of ≈5 mN/m, as being of the order of 15−300 nm. This estimate was based on the model by Evans,[51] which analyzed the variation of the free energy of biomembranes and of interlocked multilayers of lipids upon their bending deformation. Assuming zero shear resistance of the molecular layers in the multilayer structure, Evans[51] found a quadratic dependence of the bending elasticity constant, K_B, of membrane layers on their thickness h[51,52]

$$K_B \approx K_{B1}(h/h_1)^2 \tag{5}$$

where h_1 is the thickness of the contained monolayers and K_{B1} is their individual bending modulus. For frozen (rigid) monolayer of surfactant/lipid/alkane molecules with thickness $h_1 \approx 2$ nm, the bending modulus K_{B1} is in the range between 10^{-18} and 10^{-17} J.[17−19]

In his original study, Evans acknowledged[51] that the biological membranes have nonzero shear modulus, as well as suggested that the respective contribution to bending is small enough to disregard it. The scaling expressed via eq 5 has been used successfully to model numerous fluid multilayer systems.[51−54] However, the experimental results, obtained in the current study, show that the layers of plastic rotator phase are thinner and stiffer than the initial estimate proposed in refs1, 2 which calls for reconsidering the assumptions made in Evans' approach.

Considering the other extreme of bending a fully solid isotropic layer, the bending rigidity is proportional to h^3 according to the Kirchhoff−Love theory of thin elastic shells,[54] rather than to h^2, as proposed by Evans[51] and adopted by us in ref 1. The assumption that K_B is proportional to h^3 leads to the following estimate

$$h_{PL} \geq h_1(\gamma r^2/K_{B1})^{1/3} \tag{6}$$

where h_1 is the monolayer thickness, γ is the interfacial tension, r is the curvature at the droplet edges, and K_{B1} is the monolayer bending elasticity constant. Taking a high estimate, $K_{B1} \approx 10^{-17}$ J, as proposed by Guttmman et al.[17−19] and $h_1 \approx 2$ nm, yields minimum values for $h_{PL} \approx 16$ nm for $\gamma \approx 5$ mN/m and $h_{PL} \approx 7$ nm for $\gamma \approx 0.5$ mN/m. The lowest values of γ were measured with the surfactants from group A, which may explain why the respective drops could deform even with thin multilayers of rotator phase (two to three layers only). Note that the assumption for drop-shape transformation by a single monolayer requires a value of $K_{B1} \approx 10^{-16}$ J even for interfacial tension as low as $\gamma \approx 0.1$ mN/m—such a value of K_{B1} is an order of magnitude higher than the highest values reported or proposed in the literature.[17−19] Therefore, the only possibility for drop deformation by single adsorption monolayer is to have an oil−water interfacial tension of the order of 10^{-2} mN/m or lower.

We should note that it was difficult to predict which of these two models, expressed via eqs 5 or 6, would better predict the behavior of the plastic crystals without having experimental results like those obtained in the current study. We have used in our previous papers[1−3] the model by Evans and Skalak,[52] as the internal structure of the rotator phase resembles closer that of the biomembranes than that of the isotropic solid shells. As explicitly stated by Evans "...bending theory for a three-dimensional isotropic material is clearly inappropriate to lipid bilayers".[51] The direct comparison of the predictions of these two models with the current experimental results for the thickness of the rotator phase in the deformed drops allows us to conclude that the multilayers are strongly interlocked and have high shear resistance, closer to those in solid crystals. Hence, the Kirchhoff−Love model[54] describes better these results, whereas the Evans model[51] seems to overestimate the thickness of the rotator phase, despite being appropriate for describing the mechanical properties of fluid biomembranes and their multilayers.

■ CONCLUSIONS

In the current article, we present systematic and complementary DSC measurements and optical observations of the drop self-shaping phenomenon. The obtained results show unambiguously that the drop-shape transformations observed upon cooling are caused by the formation of ordered multilayers of alkane molecules at the drop surface. The thickness of the formed multilayer of rotator phase depends strongly on the type of surfactant used for emulsion stabilization and, to some extent, on the size and shape of the deformed drops.

For surfactants from group B for which $T_d \approx T_m$ (where T_m is the melting temperature of the bulk alkane), the thickness of the rotator phase varies, depending on the initial drop diameter and the drop shape. For the polyhedrons and platelets, formed

DOI: 10.1021/acs.langmuir.8b02771
Langmuir 2019, 35, 5484−5495

from 9.5 μm drops, this thickness is $h_{PL} \approx 55 \pm 15$ nm, which corresponds to $\approx 24 \pm 6$ layers of molecules. For the elongated rods formed from smaller drops, 3 μm in diameter, the thickness of the rotator phase is estimated to be $\approx$10 nm, viz., around 4 ± 1 molecular layers.

The drop transformations in the presence of surfactants from group C for which $T_d < T_m$ also induce measurable heat effects, which however overlap partially with the freezing of a small fraction of the alkane drops. From the obtained results, we could estimate the thickness of the rotator phase in these systems to be $\approx$8 nm, viz., around 3 ± 1 molecular layers.

For surfactants from group A, which induce drop-shape deformations, starting at temperature $T_d > T_m$, we could not estimate the thickness of the ordered layer because the result of this estimate depends very much on the assumptions made. By using different assumptions, we found that the thickness of the ordered layer in these systems could vary between 5 and 180 nm, which correspond to between 2 and 80 molecular layers.

The results have also allowed us to determine whether the interlayer interactions in plastic crystals are closer to those in solid crystal structures or to those in biomembranes (our original assumption in ref 1). Comparison of the model predictions to the obtained results allowed us to conclude that the measured thickness of the rotator phase is better described by the Kirchoff–Love theory of thin elastic shells[54] predicting $K_B \propto h_{PL}^3$, where K_B is the bending elastic modulus and h_{PL} is the thickness of the plastic rotator phase, formed on the drop surface. This information will be used to develop the thermodynamic model able to explain the self-shaping phenomenon.

The obtained results provide directions for the optimization and rational control of the processes of drop self-shaping in the various systems and on the related process of drop bursting (self-emulsification) observed[7,8] in some of these emulsions.

■ ASSOCIATED CONTENT

Supporting Information

The Supporting Information is available free of charge on the ACS Publications website at DOI: 10.1021/acs.langmuir.8b02771.

Properties of the alkanes studied (Table S1); properties and structural formulas of surfactants (Table S2); surfactant classification (Table S3); drop-shape evolutionary scheme (Figure S1); experimental setup for optical observations (Figures S2 and S3); histograms of the drop-size distributions (Figure S4); microscopy images for Group D (Figure S5); cooling thermograms (Figures S6, S7, S9, and S10); heating thermograms (Figure S8); geometric models for tetragonal platelets (Figures S11, S12 and S13); and two geometric models for Group A (Figure S14) (PDF)

Formation of corrugated polyhedrons and several subsequent breakage events observed upon cooling of emulsion system from Group A (AVI)

■ AUTHOR INFORMATION

Corresponding Author

*E-mail: nd@lcpe.uni-sofia.bg. Tel: +359 2 8161639. Fax: +359 2 9625643.

ORCID

Nikolai Denkov: 0000-0003-1118-7635

Slavka Tcholakova: 0000-0001-8091-7529

Stoyan K. Smoukov: 0000-0003-1738-818X

Notes

The authors declare no competing financial interest.

■ ACKNOWLEDGMENTS

This work was funded by the European Research Council (ERC) grant to Stoyan Smoukov, EMATTER (#280078). The study falls under the umbrella of European networks COST MP1305 and MP1106. Z.V. is grateful for the financial support provided for the execution of STSM project: Cost-STSM-MP1305-30666, and D.C. for the financial support for execution of STSM project: Cost-STSM-MP1106-071867, allowing them to become familiar with the DSC technique and to obtain important experimental results. Useful discussions with Dr. Ivan Lesov are gratefully acknowledged.

■ REFERENCES

(1) Denkov, N.; Tcholakova, S.; Lesov, I.; Cholakova, D.; Smoukov, S. K. Self-shaping of oil droplets via the formation of intermediate rotator phases upon cooling. *Nature* **2015**, *528*, 392–395.

(2) Cholakova, D.; Denkov, N. D.; Tcholakova, S.; Lesov, I.; Smoukov, S. K. Control of drop shape transformations in cooled emulsions. *Adv. Colloid Interface Sci.* **2016**, *235*, 90–107.

(3) Denkov, N.; Cholakova, D.; Tcholakova, S.; Smoukov, S. K. On the mechanism of drop self-shaping in cooled emulsions. *Langmuir* **2016**, *32*, 7985–7991.

(4) Cholakova, D.; Valkova, Z.; Tcholakova, S.; Denkov, N.; Smoukov, S. K. "Self-shaping" of multicomponent drops. *Langmuir* **2017**, *33*, 5696–5706.

(5) Lesov, I.; Valkova, Z.; Vassileva, E.; Georgiev, G.; Ruseva, K.; Simeonov, M.; Tcholakova, S.; Denkov, N.; Smoukov, S. Bottom-up synthesis of polymeric micro- and nanoparticles with regular anisotropic shapes. *Macromolecules* **2018**, *51*, 7456–7462.

(6) Gordon, R.; Hanczyc, M.; Denkov, N.; Tiffany, M.; Smoukov, S. K. Emergence of polygonal shapes in oil droplets and living cells: The potential role of tensegrity in the origin of life. In *Habitability of the Universe before Earth*; Academic Press, 2018; pp 427–490.

(7) Tcholakova, S.; Valkova, Z.; Cholakova, D.; Vinarov, Z.; Lesov, I.; Denkov, N.; Smoukov, S. K. Efficient self-emulsification via cooling-heating cycles. *Nat. Commun.* **2017**, *8*, No. 15012.

(8) Valkova, Z.; Cholakova, D.; Tcholakova, S.; Denkov, N.; Smoukov, S. K. Mechanisms and control of self-emulsification upon freezing and melting of dispersed alkane drops. *Langmuir* **2017**, *33*, 12155–12170.

(9) Small, D. M. *The Physical Chemistry of Lipids. From Alkanes to Phospholipids*; Plenum: New York, 1986.

(10) Sirota, E.; King, H.; Singer, D.; Shao, H. Rotator phases of the normal alkanes: An x-ray scattering study. *J. Chem. Phys.* **1993**, *98*, 5809–5824.

(11) Sirota, E.; Singer, D. Phase transitions among the rotator phases of the normal alkanes. *J. Chem. Phys.* **1994**, *101*, 10873–10882.

(12) Sirota, E.; Herhold, A. Transient phase-induced nucleation. *Science* **1999**, *283*, 529–532.

(13) Ueno, S.; Hamada, Y.; Sato, K. Controlling polymorphic crystallization of n-alkane crystals in emulsion droplets through interfacial heterogeneous nucleation. *Cryst. Growth Des.* **2003**, *3*, 935–939.

(14) Shinohara, Y.; Takamizawa, T.; Ueno, S.; Sato, K.; Kobayashi, I.; Nakajima, M.; Amemiya, Y. Microbeam X-Ray diffraction analysis of interfacial heterogeneous nucleation in n-hexadecane inside oil-in-water emulsion droplets. *Cryst. Growth Des.* **2008**, *8*, 3123–3126.

(15) Shinohara, Y.; Kawasaki, N.; Ueno, S.; Kobayashi, I.; Nakajima, M.; Amemiya, Y. Observation of the transient rotator phase of n-hexadecane in emulsified droplets with time-resolved two-dimensional small- and wide-angle X-Ray scattering. *Phys. Rev. Lett.* **2005**, *94*, No. 097801.

DOI: 10.1021/acs.langmuir.8b02771
Langmuir 2019, 35, 5484–5495

(16) Cholakova, D. Control of the shape of emulsion droplets undergoing phase transition (in Bulgarian), Bachelor's Degree Thesis, supervisor Prof. N. Denkov, reviewer Dr. K. Golemanov, 2016.
(17) Guttman, S.; Sapir, Z.; Schultz, M.; Butenko, A.; Ocko, B.; Deutsch, M.; Sloutskin, E. How faceted liquid droplets grow tails. *Proc. Natl. Acad. Sci. USA* **2016**, *113*, 493−496.
(18) Guttman, S.; Ocko, B.; Deutsch, M.; Sloutskin, E. From faceted vesicles to liquid icoshedra: Where topology and crystallography meet. *Curr. Opin. Colloid Interface Sci.* **2016**, *22*, 35−40.
(19) Guttman, S.; Sapir, Z.; Ocko, B.; Deutsch, M.; Sloutskin, E. Temperature-tuned faceting and shape changes in liquid alkane droplets. *Langmuir* **2017**, *33*, 1305−1314.
(20) Höhne, G.; Hemminger, W.; Flammersheim, H. *Differential Scanning Calorimetry*; Springer, 2003.
(21) Günther, E.; Hiebler, S.; Mehling, H.; Redlich, R. Enthalpy of phase change materials as a function of temperature required accuracy and suitable measurement methods. *Int. J. Thermophys.* **2009**, *30*, 1257−1269.
(22) Gill, P.; Moghadam, T.; Ranjbar, B. Differential scanning calorimetry techniques: applications in biology and nanoscience. *J. Biomol. Tech.* **2010**, *21*, 167−193.
(23) Clas, S.-D.; Dalton, C.; Hancock, B. Differential scanning calorimetry: applications in drug development. *Pharm. Sci. Technol. Today* **1999**, *2*, 311−320.
(24) Bruylants, G.; Wouters, J.; Michaux, C. Differential scanning calorimetry in life science: Thermodynamics, stability molecular recognition and application in drug design. *Curr. Med. Chem.* **2005**, *12*, 2011−2020.
(25) Spink, C. Differential scanning calorimetry. *Methods Cell Biol.* **2008**, *84*, 115−141.
(26) Biliaderis, C. Differential scanning calorimetry in food research − A review. *Food Chem.* **1983**, *10*, 239−265.
(27) Slade, L.; Levine, H. Glass transitions and water-food structure interactions. *Adv. Food Nutr. Res.* **1995**, *38*, 103−269.
(28) Nishinari, K. Rheological and DSC study of sol-gel transition in aqueous dispersions of industrially important polymers and colloids. *Colloid Polym. Sci.* **1997**, *275*, 1093.
(29) Johnson, C. Differential scanning calorimetry as a tool for protein folding and stability. *Arch. Biochem. Biophys.* **2013**, *531*, 100−109.
(30) Demetzos, C. Differential scanning calorimetry (DSC): A tool to study the thermal behavior of lipid bilayers and liposomal stability. *J. Liposome Res.* **2008**, *18*, 159−173.
(31) Vélez, C.; Khayet, M.; Ortiz de Zarate, J. M. Temperature-dependent thermal properties of solid/liquid phase change even-numbered n-alkanes: n-hexadecane, n-octadecane and n-eicosane. *Appl. Energy* **2015**, *143*, 383−394.
(32) Knothe, G.; Dunn, R. A comprehensive evaluation of the melting points of fatty acids and esters determined by differential scanning calorimetry. *J. Am. Oil Chem. Soc.* **2009**, *86*, 843−856.
(33) Clausse, D. Differential thermal analysis, differential scanning calorimetry, and emulsions. *J. Therm. Anal. Calorim.* **2010**, *101*, 1071−1077.
(34) Clausse, D.; Gomez, F.; Pezron, I.; Komunjer, L.; Dalmazzone, C. Morphology characterization of emulsions by differential scanning calorimetry. *Adv. Colloid Interface Sci.* **2005**, *117*, 59−74.
(35) Dalmazzone, C.; Noik, C.; Clausse, D. Application of DSC for emulsified system characterization. *Oil Gas Sci. Technol.* **2009**, *64*, 543−555.
(36) Potier, L.; Raynal, S.; Seiller, M.; Grossiord, J.-L.; Clausse, D. Study of state transitions within multiple w/o/w emulsions using calorimetry (DSC). *Thermochim. Acta* **1992**, *204*, 145−155.
(37) Palanuwech, J.; Coupland, J. Effect of surfactant type on the stability of oil-in-water emulsions to dispersed phase crystallization. *Colloids Surf., A* **2003**, *223*, 251−262.
(38) Gülseren, İ.; Coupland, J. Excess ultrasonic attenuation due to solid-solid and solid-liquid transitions in emulsified octadecane. *Cryst. Growth Des.* **2007**, *7*, 912−918.
(39) McClements, D. J.; Dungan, S.; German, J.; Simoneau, C.; Kinsella, J. Droplet size and emulsifier type affect crystallization and melting of hydrocarbon-in-water emulsions. *J. Food Sci.* **1993**, *58*, 1148−1178.
(40) Gülseren, İ.; Coupland, J. Surface melting in alkane emulsion droplets as affected by surfactant type. *J. Am. Oil Chem. Soc.* **2008**, *85*, 413−419.
(41) Xie, B.; Liu, G.; Jiang, S.; Zhao, Y.; Wang, D. Crystallization behaviors of *n*-octadecane in confined space: Crossover of rotator phase from transient to metastable induced by surface freezing. *J. Phys. Chem. B* **2008**, *112*, 13310−13315.
(42) Kandori, K., Gaonkar, A., Ed. *Applications of Microporous Glass Membranes: Membrane Emulsification*; Elsevier, 1995; Chapter 7, pp 113−142.
(43) Charcosset, C.; Limayem, I.; Fessi, H. The membrane emulsification process − a review. *J. Chem. Technol. Biotechnol.* **2004**, *79*, 209−218.
(44) Christov, N.; Ganchev, D.; Vassileva, N.; Denkov, N.; Danov, K.; Kralchevsky, P. Capillary mechanisms in membrane emulsification: oil-in-water emulsions stabilized by Tween 20 and milk proteins. *Colloids Surf. A* **2002**, *209*, 83−104.
(45) Nakashima, T.; Shimizu, M.; Kukizaki, M. Membrane emulsification by microporous glass. *Key Eng. Mater.* **1992**, *61−62*, 513−516.
(46) Svarovsky, L. *Solid-Liquid Separation*, 4th ed.; Butterworth-Heinemann, 2000.
(47) Newton, R. H.; Haffegee, J. P.; Ho, M. H. Polarized light microscopy of weakly birefringent biological specimens. *J. Microsc.* **1995**, *180*, 127−130.
(48) Holmberg, K. *Handbook of Applied Surface and Colloid Chemistry*. Identification of Lyotropic Liquid Crystalline Mesophases; John Wiley & Sons, 2001; pp 299−332, Vol. 2, Chapter 16.
(49) Tokiwa, Y.; Sakamoto, H.; Takiue, T.; Aratono, M.; Matsubara, H.; Bain, C. Effect of surface freezing on stability of oil-in-water emulsions. *Langmuir* **2018**, *34*, 6205−6209.
(50) Mondieig, D.; Rajabalee, F.; Metivaud, V.; et al. n-Alkane Binary Molecular Alloys. *Chem. Mater.* **2004**, *16*, 786−798.
(51) Evans, E. A. Bending Resistance and Chemically Induced Moments in Membrane Bilayers. *Biophys. J.* **1974**, *14*, 923−931.
(52) Evans, E.; Skalak, R. *Mechanics and Thermodynamics of Biomembranes*; CRC, 1980.
(53) Bermúdez, H.; Hammer, D. A.; Discher, D. E. Effect of Bilayer Thickness on Membrane Bending Rigidity. *Langmuir* **2004**, *20*, 540−543.
(54) Love, A. E. H. The small free vibrations and deformation of a thin elastic shell. *Philos. Trans. R. Soc., A* **1888**, *179*, 491.

DOI: 10.1021/acs.langmuir.8b02771
Langmuir 2019, 35, 5484−5495